Numerical study of the meta-nanopyramid array as efficient solar energy absorber

Qiuqun Liang,[1,2] Weixing Yu,[1,4,*] Wencai Zhao,[1] Taisheng Wang,[1] Jingli Zhao,[1] Hongsheng Zhang,[1] and Shaohua Tao[3,4,5]

[1]*State Key Laboratory of Applied Optics, Changchun Institute of Optics, Fine mechanics and Physics, Chinese Academy of Sciences, 3888 Dongnanhu Road, Changchun, Jilin, 130033, China*
[2]*University of Chinese Academy of Sciences, Beijing, 100039, China*
[3] *Institute of Super Microstructure and Ultrafast Process, School of Physics and Electronics, Central South University, Changsha, Hunan 410083, China*
[4]*These two authors contributed equally to the paper*
[5]*eshtao@esu.edu.cn*
[*]*yuwx@ciomp.ac.cn*

Abstract: Conventional dielectric moth eye structure is well known to be antireflective, but cannot work well in the whole solar spectrum. In addition, it cannot be used as a light absorber. However, in some cases, light absorbing and harvesting are important for energy conversion from light to heat or electricity. Here, we propose a metamaterial-based nanopyramid array which shows near 100% absorbing property in the entire solar spectrum (i.e. 0.2-2.5 μm). In addition, the high absorption performance of meta-nanopyramid array retains very well at a wide receiving angle with polarization-independent. Thus, it can dramatically improve the efficiency of the solar light absorbing. The efficient light absorbing property can be explained in terms of the synergetic effects of slow light mode, surface plasmon polariton resonance and magnetic polariton resonance.

OCIS codes: (240.6680) Surface plasmons; (160.3918) Metamaterials; (260.5740) Resonance; (310.6628) Subwavelength structures, nanostructures.

References and links

1. D. S. Hobbs, B. D. MacLeod, and J. R. Riccobono, "Update on the development of high performance anti-reflecting surface relief microstructures," Proc. SPIE **6545**, 65450Y, 65450Y-14 (2007).
2. S. Wilson and M. Hutley, "The optical properties of 'moth eye' antireflection surfaces," J. Mod. Opt. **29**(1), 993–1009 (1982).
3. D. Stavenga, S. Foletti, G. Palasantzas, and K. Arikawa, ""Light on the moth-eye corneal nipple array of butterflies," P. Roy.Soc. B-Biol," Sci. **273**(1587), 661–667 (2006).
4. S. J. Choi and S. Y. Huh, "Direct structuring of a biomimetic anti-reflective, self-cleaning surface for light harvesting in organic solar cells," Macromol. Rapid Commun. **31**(6), 539–544 (2010).
5. R. Brunner, O. Sandfuchs, C. Pacholski, C. Morhard, and J. Spatz, "Lessons from nature: biomimetic subwavelength structures for high-performance optics," Laser. Photonics. Rev **6**(5), 641–659 (2012).
6. R. Dewan, S. Fischer, V. B. Meyer-Rochow, Y. Özdemir, S. Hamraz, and D. Knipp, "Studying nanostructured nipple arrays of moth eye facets helps to design better thin film solar cells," Bioinspir. Biomim. **7**(1), 016003 (2012).
7. J. S. Y. Young Min Song and Y. T. Lee, "Antireflective submicrometer gratings on thin-film silicon solar cells for light-absorption enhancement," Opt. Lett. **35**(3), 226–228 (2010).
8. P. Clapham and M. Hutley, "Reduction of lens reflection by the "moth eye" principle," Nature **244**(5414), 281–282 (1973).
9. S. Chattopadhyay, Y. Huang, Y. Jen, A. Ganguly, K. Chen, and L. Chen, "Anti-reflecting and photonic nanostructures," Mater. Sci. Eng. Rep. **69**(1), 1–35 (2010).
10. J. B. Pendry, "Negative refraction makes a perfect lens," Phys. Rev. Lett. **85**(18), 3966–3969 (2000).
11. D. Schurig, J. J. Mock, B. J. Justice, S. A. Cummer, J. B. Pendry, A. F. Starr, and D. R. Smith, "Metamaterial electromagnetic cloak at microwave frequencies," Science **314**(5801), 977–980 (2006).
12. N. Fang, H. Lee, C. Sun, and X. Zhang, "Sub-diffraction-limited optical imaging with a silver superlens," Science **308**(5721), 534–537 (2005).
13. J. Valentine, S. Zhang, T. Zentgraf, E. Ulin-Avila, D. A. Genov, G. Bartal, and X. Zhang, "Three-dimensional optical metamaterial with a negative refractive index," Nature **455**(7211), 376–379 (2008).
14. X. He, Y. Wang, J. Wang, T. Gui, and Q. Wu, "Dual-band terahertz metamaterial absorber with polarization insensitivity and wide incident angle," Prog. Electromagnetics Res. **115**, 381–397 (2011).

#190965 - $15.00 USD Received 24 May 2013; revised 11 Jul 2013; accepted 11 Jul 2013; published 29 Jul 2013

15. C. W. Cheng, M. N. Abbas, C. W. Chiu, K. T. Lai, M. H. Shih, and Y. C. Chang, "Wide-angle polarization independent infrared broadband absorbers based on metallic multi-sized disk arrays," Opt. Express **20**(9), 10376–10381 (2012).
16. D. Cheng, J. Xie, H. Zhang, C. Wang, N. Zhang, and L. Deng, "Pantoscopic and polarization-insensitive perfect absorbers in the middle infrared spectrum," JOSA B **29**(6), 1503–1510 (2012).
17. Y. Ye, Y. Jin, and S. He, "Omnidirectional, polarization-insensitive and broadband thin absorber in the terahertz regime," JOSA B **27**(3), 498–504 (2010).
18. C. Hu, Z. Zhao, X. Chen, and X. Luo, "Realizing near-perfect absorption at visible frequencies," Opt. Express **17**(13), 11039–11044 (2009).
19. Q. Liang, T. Wang, Z. Lu, Q. Sun, Y. Fu, and W. Yu, "Metamaterial-based two dimensional plasmonic subwavelength structures offer the broadest waveband light harvesting," Adv. Opt. Mater. **1**(1), 43–49 (2013).
20. K. Liou, An introduction to atmospheric radiation, **84** (Academic press, 2002).
21. FDTD, lumerical, http://www.lumerical.com/, 10, 2010.
22. E. Palik, Handbook of optical constants of solids, **3** (Academic press, 1998).
23. J. Dobrowolski, "Optical properties of films and coatings," Handbook of Optics 1, 42–1 (1995).
24. T. C. Choy, *Effective Medium Theory: Principles and Applications*, **102** (Oxford University Press on Demand, 1999).
25. D. Aspnes, "Local-field effects and effective-medium theory: A microscopic perspective," Am. J. Phys. **50**(8), 704–709 (1982).
26. T. Tang, F. Chen, and B. Sun, "Photonic band gap from periodic structures containing anisotropic nonmagnetic left-handed metamaterial," Chin. Opt. Lett. **8**(4), 431–434 (2010).
27. D. R. Smith, D. C. Vier, T. Koschny, and C. M. Soukoulis, "Electromagnetic parameter retrieval from inhomogeneous metamaterials," Phys. Rev. E Stat. Nonlin. Soft Matter Phys. **71**(3 3 Pt 2B), 036617 (2005).
28. L. Huang and H. Chen, "Multi-band and polarization insensitive metamaterial absorber," Prog. Electromagnetics Res. **113**, 103–110 (2011).
29. X. Chen, T. M. Grzegorczyk, B.-I. Wu, J. Pacheco, Jr., and J. A. Kong, "Robust method to retrieve the constitutive effective parameters of metamaterials," Phys. Rev. E Stat. Nonlin. Soft Matter Phys. **70**(1), 016608 (2004).
30. J. He and S. He, "Slow propagation of electromagnetic waves in a dielectric slab waveguide with a left-handed material substrate," IEEE Microw. Wirel. Co **16**(2), 96–98 (2006).
31. Y. Cui, K. H. Fung, J. Xu, H. Ma, Y. Jin, S. He, and N. X. Fang, "Ultrabroadband light absorption by a sawtooth anisotropic metamaterial slab," Nano Lett. **12**(3), 1443–1447 (2012).
32. N. Liu, L. Fu, S. Kaiser, H. Schweizer, and H. Giessen, "Plasmonic building blocks for magnetic molecules in three-dimensional optical metamaterials," Adv. Mater. **20**(20), 3859–3865 (2008).
33. H. Raether, Surface plasmons (Springer-Verlag Berlin, 1988).
34. Y. Cheng, Y. Nie, and R. Gong, "A polarization-insensitive and omnidirectional broadband terahertz metamaterial absorber based on coplanar multi-squares films," Opt. Laser Technol. **48**, 415–421 (2013).
35. W. Cai, U. K. Chettiar, H. K. Yuan, V. C. de Silva, A. V. Kildishev, V. P. Drachev, and V. M. Shalaev, "Metamagnetics with rainbow colors," Opt. Express **15**(6), 3333–3341 (2007).
36. H. Tao, N. I. Landy, C. M. Bingham, X. Zhang, R. D. Averitt, and W. J. Padilla, "A metamaterial absorber for the terahertz regime: design, fabrication and characterization," Opt. Express **16**(10), 7181–7188 (2008).

1. Introduction

It is well known that when the electromagnetic wave hits the interface of two different media, it may be reflected, transmitted, scattered, absorbed or excite surface electromagnetic waves. Obviously, it is a big challenge to find a solid material that matches the refractive index of air. Therefore, much attention has been paid to antireflection (AR) coating. Solar cells, which harvest solar energy directly from sunlight and convert it into electricity, have been attracting much attention for decades, and most of the existing solar cells are employing the antireflection (AR) coating to improve their quantum efficiency. Typically, there are two types of AR coating. One is homogeneous AR coating, and the other is inhomogeneous AR coating. Homogeneous antireflection coating consisting of multilayer quarter wavelength anti-reflection thin films reduces the reflection by the destructive interference of light at different interfaces. However, the bandwidth of these coating is generally narrower than one octave (e.g. 400-700 nm or 800-1100 nm, 1.5-1.6 μm, 3-5 μm, 8-12 μm) and the effective receiving angle of light is less than 30° [1]. Inhomogeneous antireflection coating is also called gradient refractive index coating and the refractive index of the coating is gradually increased from the value of the ambient air to that of the bulk material (i.e. substrate), as the filling factor of the material is gradually increased [2]. The variation of refractive index follows several profiles (linear, cubic, parabolic, quintic etc.). The reflection is effectively reduced due to the elimination of the abrupt change of the refractive index and the optical impedance matching at the interfaces. The advantage of the graded refractive index coating is that its antireflective

#190965 - $15.00 USD Received 24 May 2013; revised 11 Jul 2013; accepted 11 Jul 2013; published 29 Jul 2013

property retains in omni-direction with wide incident angles. Many efforts have been made over decades to obtain graded index coating. Biological structures such as moth eyes have attracted lots of attentions. Conventional inhomogeneous AR coatings (moth eye structures) are composed of continuous homogeneous dielectrics. They exhibit ultralow reflection in broad waveband with omni-directional light incidences [2–8]. The reduction of specular reflectance in the dielectric moth eye structure is not due to the increase in diffuse scattering or the degradation of transmitted wavefront, but solely the consequence of enhanced transmission [2,9]. To be an absorber, however, a thick opaque metallic ground plane is often added to the bottom of the structure to block any transmission. Thus, the continuous homogeneous dielectrics like the biomimetic moth-eye structure cannot be used as a broadband absorber.

Metamaterials are artificial materials composed of patterned metallic/dielectric subwavelength micro/nanostructures and their electromagnetic properties can be tuned by engineering the geometry. For their exotic electromagnetic responses, such as negative refractive index, superlensing and cloaking, are not readily available in nature, metamaterials have recently attracted considerable attentions [10–13]. Metamaterial-based absorber has been reported to be able to obtain near 100% absorption in the THz region, infrared region and visible region [14–18]. Our previous study has shown that the two-dimensional pyramidal shape metamaterial-based absorber is a broadband, wide-angle, omni-directional and polarization-insensitive light absorbing device with an absorption of nearly 100% in the infrared waveband from 1 μm to 14 μm [19]. In this paper, we numerically investigate the absorption performance and the absorption mechanism of the proposed metamaterial-based nanopyramidal absorber in the entire solar spectrum (0.2-2.5 μm) [20].

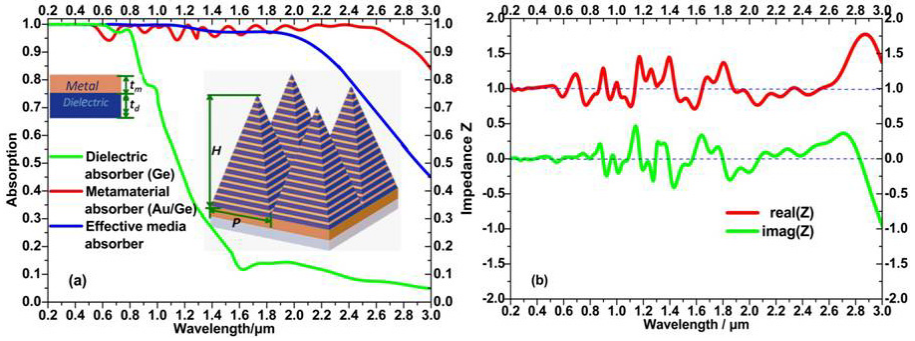

Fig. 1. (a) Calculated absorption spectra of the dielectric absorber, metamaterial-based nanopyramidal solar energy absorber and the effective homogeneous pyramidal structure with the same period (P) and height (H): P = 200 nm, H = 510 nm. (b) Retrieved impedance Z of the metamaterial-based nanopyramidal solar energy absorber. The insets of Fig. 1(a) show the diagram of metamaterial-based nanopyramidal solar energy absorber. The thickness of metal film(t_m) and dielectric film (t_d) is t_m = 10 nm and t_d = 20 nm respectively. The number of metal/dielectric pairs N = 17.

2. Metamaterial-based nanopyramidal efficient solar energy absorber

Our proposed metamaterial-based nanopyramidal structure is composed of alternating metallic (gold) and dielectric (germanium) multi-layer thin films and a bottom metallic mirror (gold) as shown in the insets of Fig. 1(a). The optimized metamaterial-based nanopyramidal structure was obtained through Finite-Difference Time-Domain (FDTD) simulations (Lumerical Inc.) [21]. The three-dimensional simulations were performed with a plane wave source incident in the z direction. Periodic boundary conditions were employed for both x and y directions with a mesh step size of Δx=Δy=5 nm, and a perfect matching layer boundary condition was employed in z direction with a mesh step size of Δz=2 nm. The material properties of gold and germanium were chosen from the software database-Au (Gold) Palik, Ge (Germanium)-Palik [22]. The absorption spectra were obtained using the formula A(λ)=1-

#190965 - $15.00 USD Received 24 May 2013; revised 11 Jul 2013; accepted 11 Jul 2013; published 29 Jul 2013

R(λ)-T(λ), where $R(\lambda)=|S_{11}|^2$ is the reflection and $T(\lambda)=|S_{21}|^2$ is the transmission. Since the thickness of the bottom ground metal plane (t = 100 nm) is much larger than its typical skin depth, the transmission is suppressed in overall spectral range ($T(\lambda)=|S_{21}|^2=0$).

The thickness of the metal and dielectric films should be optimized to achieve impedance matching so that the maximum absorption can be obtained. As for the thickness of the metal film, it should be close to its skin depth so that the incident light is allowed to be able to penetrate through the metal film directly. Since the skin depth of the gold is about 10nm in the waveband considered, the thickness of the gold film is taken as t_m = 10 nm. On the other hand, the thickness of the dielectric film also has effect on the absorption performance, because it influences the light interaction between the adjacent metal films. For the convenience of the fabrication, the thickness of the metal film should not be too thin. In the metamaterial-based nanopyramidal infrared absorber, the optimized thickness of the dielectric film (germanium) is about 190 nm, with the period of the nanopyramid array equaling to 1.6 μm [16]. However, such a thick dielectric film does not result in efficient absorption in the spectrum considered here. In order to have a good absorption performance in the overall solar spectrum, thinner dielectric layer is required as the period of the pyramidal meta-structures is much smaller (reduced from 1.6 μm to 0.2 μm). The optimized thickness of germanium film is about 20 nm for the period 200 nm. The total number of metal/dielectric pairs (N) is 17. The period of the pyramid array is 200 nm in both x and y directions. The absorption spectrum at normal incidence (shown in Fig. 1(a) red line) indicates that the designed structure has an absorptivity of nearly 100% at the waveband 0.2-2.6 μm, which covers the whole solar irradiance spectrum (0.2-2.5 μm). This indicates that the designed pyramidal meta-nanostructure is a perfect solar energy absorber. Moreover, the longest wavelength λ_U to the shortest wavelength λ_L in the working waveband is very large, i.e. $|\lambda_U/\lambda_L| = 13$. In contrast, AR coating designs typically fail in spectral ranges $0.85 < \{|\lambda_U/\lambda_L|\} < 5$ [23]. In addition, the absorption of the continuous homogeneous dielectric nanopyramidal structure normally can only achieve near unity absorption in a very narrow waveband of 200-800 nm for germanium nanopyramidal structure (as shown by the green line in Fig. 1(a)). Thus, one can see that by using the metamaterial, the absorption spectrum is significantly expanded and can cover the entire solar spectrum.

According to the effective medium theory, the meta-nanopyramid arrays can be regarded as homogeneous materials with anisotropic permittivity, and can be described as metamaterials with effective constitutive parameters [24–26]. The effective permittivity model of components $\varepsilon_{//}$ and $\varepsilon_{\perp}$ for the metamaterial is related to the relative permittivity of gold ε_m and germanium ε_d, which can be described by [24,25],

$$\varepsilon_{//} = f\varepsilon_m(\omega) + (1-f)\varepsilon_d(\omega) \tag{1}$$

and

$$\frac{1}{\varepsilon_{\perp}} = \frac{f}{\varepsilon_m(\omega)} + \frac{1-f}{\varepsilon_d(\omega)} \tag{2}$$

where f is the filling ratio of the metal film. One can find that the absorption spectrum of the effective pyramidal structure (Fig. 1(a), blue line) is very similar to that of the actual metamaterial pyramidal structure (Fig. 1(a), red line). However, a large discrepancy exists in between two spectral curves for those wavelengths larger than 2.0 μm. This could be attributed to that the effective permittivity model presented above is not accurate enough when the wavelength is larger than 2 μm for this kind of structure.

Moreover, both the real and imaginary parts of the retrieved effective impedance $\tilde{z}$ of the proposed metamaterial-based absorber are calculated by using S-parameter retrieval algorithm [27]:

$$\tilde{z} = \sqrt{\frac{(1+S_{11})^2 - S_{21}^2}{(1-S_{11})^2 - S_{21}^2}} \tag{3}$$

#190965 - $15.00 USD Received 24 May 2013; revised 11 Jul 2013; accepted 11 Jul 2013; published 29 Jul 2013

It is obvious from Fig. 1(b) that the real relative impedance is near unity, i.e. $\mathrm{Re}(\tilde{z}) \approx 1$, which means that $\tilde{z} \approx \tilde{z}_0 = 1$ (where $\tilde{z}_0$ is the impedance of the free space). While the imaginary part is $\mathrm{Im}(\tilde{z}) \approx 0$, which means that the reflection and the transmission are nearly zero. And thus, the proposed solar energy absorber has impedance nearly matched to that of the free space in the waveband 0.2-2.5 μm. Since S_{21}=0 is for the entire frequency band, the effective refractive index of the metamaterial-based absorber cannot be accurately calculated by the retrieval algorithm. But one can roughly estimate it from the relation between the refractive index and the scattering parameters by the following equation [28,29],

$$e^{ink_0 d} = S_{21} / (1 - S_{11} \frac{\tilde{z} - 1}{\tilde{z} + 1}) \tag{4}$$

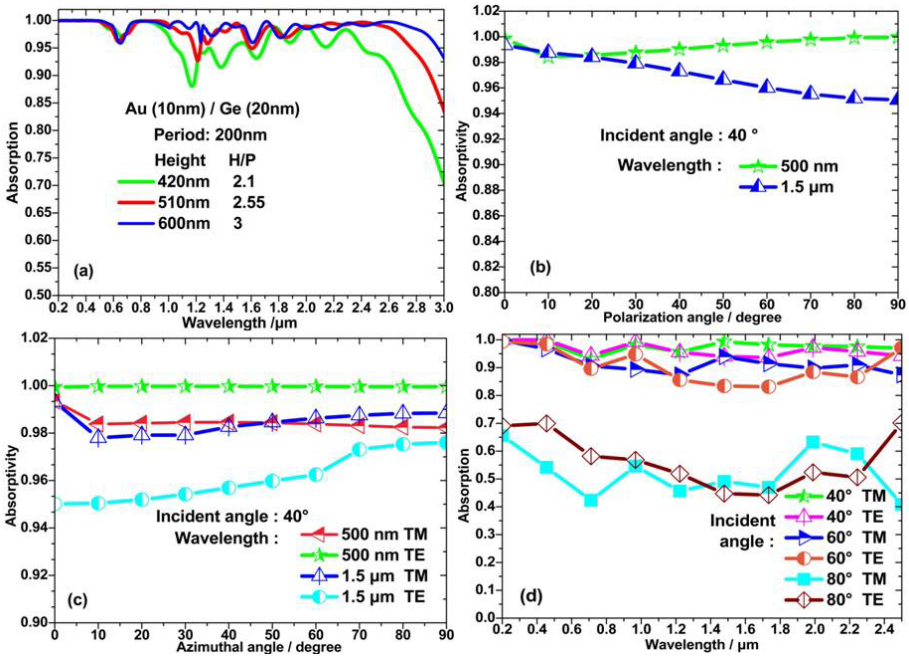

Fig. 2. (a) Absorption spectra of the metamaterial-based nanopyramidal solar energy absorber with different height of the nanopyramid, when the period of the nanopyramid array is 200 nm. (b) Absorption spectra as a function of polarization angle; (c) Absorption spectra as a function of azimuthal angle, when the incident angle θ = 40° and the wavelength λ_0 = 500 nm, and 1.5 μm, respectively. (d) Absorption spectra for different oblique incident angles: θ = 40°, 60°, and 80°, respectively, when azimuthal angle φ = 0. The period (P) and height (H) of the metamaterial-based nanopyramidal solar energy absorber in Fig. 2. (b) , (c) and (d) are: P = 200 nm, H = 510 nm.

Since the right side of the equation is zero (S_{21}=0), the imaginary part of the refractive index should be very large, so as to make the left side of the equation to be zero, too. The very large imaginary part of the refractive index gives rise to a very high absorption, thus the incident wave is totally absorbed by the metamaterial-based absorber.

It is worth mentioning that the period (P) of the nanopyramid array is chosen as 200 nm to make the designed structure to be a subwavelength structure for the operating waveband. The height (H) of the nanopyramid is optimized to be 510 nm, the minimum to grantee a near 100% absorbing in the operating waveband. Apparently, the higher the nanopyramid is, the better the light absorption is, as shown in Fig. 2(a). And a high aspect ratio about 2.5 is required to have near unity absorption in the entire spectrum considered. In addition, the designed absorber is almost insensitive to the polarization and the azimuth of the incident wave due to the four-fold symmetrical pyramidal structure. Figures 2(b) and 2(c) show the

#190965 - $15.00 USD Received 24 May 2013; revised 11 Jul 2013; accepted 11 Jul 2013; published 29 Jul 2013

performances of the metamaterial-based absorber for different polarizations and different azimuthal angles of the incident wave, respectively. Here we only show the cases when λ_0 = 500 nm and 1.5 μm. The absorption spectra at various oblique angles for TM wave and TE wave were also numerically studied, as is shown in Fig. 2(d). In the simulations of oblique incidence cases, Bloch boundary conditions in both x and y directions are employed, while maintaining all other aforementioned parameters unchanged. It is evident from Fig. 2(d) that the absorption retains up to 80% over a wide incident angle of 60° for both TM and TE waves, with an average about 95% for TM wave and 90% for TE wave. All these simulation results indicate that the designed absorber is polarization-independent and omni-directional, with a wide incident angle.

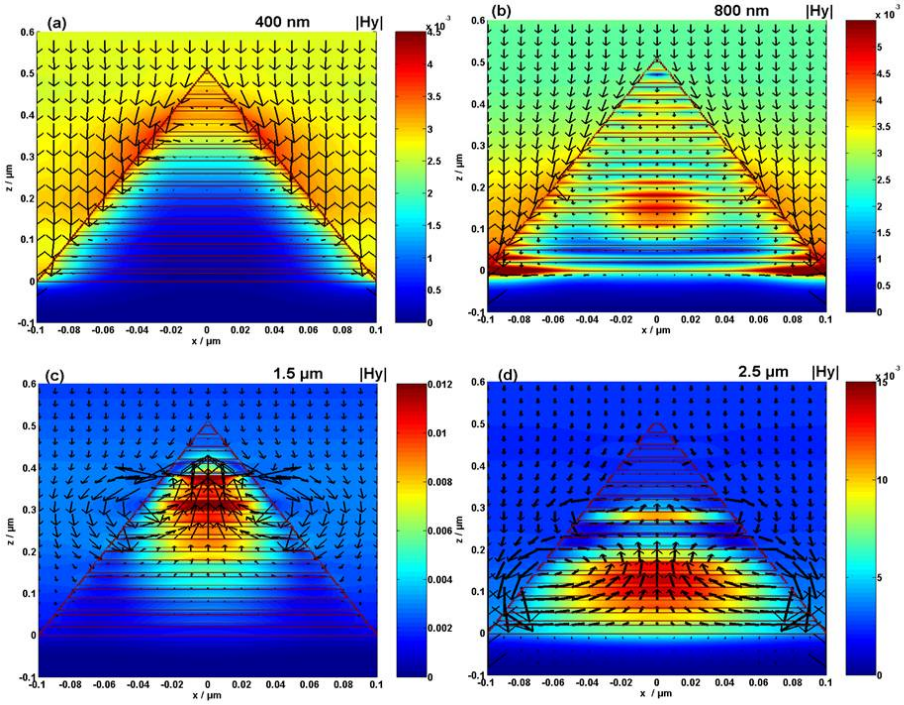

Fig. 3. Distributions of the y-component magnetic field ($|H_y|$) (color maps) and the energy flow (arrow maps) of the metamaterial-based nanopyramidal solar energy absorber in the plane $y = 0$ at four different TM waves λ_0: (a) 400 nm, (b) 800 nm, (c) 1.5 μm, and (d) 2.5 μm, respectively. The incident wavelength for each case is shown at the top right side of each figure.

3. Numerical investigation of the absorption mechanism

To better understand the absorption mechanism of the proposed metamaterial-based nanopyramidal solar energy absorber, the distributions of the y-component magnetic field ($|H_y|$) and the energy flow in the plane $y = 0$ of the proposed metamaterial-based absorber at several incident wavelengths (400 nm, 800 nm, 1.5 μm and 2.5 μm) with TM polarization are depicted in Fig. 3. Interestingly enough, for those wavelengths larger than 800 nm (at which the dielectric nanopyramidal structure cannot perform well), the metamaterial-based absorber exhibits slow light modes [30,31], which can be seen from the plots of the Poynting vectors (S) depicted in Fig. 3 by the black arrows, suggesting a significant light trapping effect. The incident energy whirls into the designed structures exactly at the positions where the magnetic fields with great enhancement are concentrated. Thus, the total energy is collected in the metamaterial-based absorber. Great enhancement of the magnetic field excited in the metamaterial-based absorber indicates the excitation of the magnetic polaritons and the

#190965 - $15.00 USD Received 24 May 2013; revised 11 Jul 2013; accepted 11 Jul 2013; published 29 Jul 2013

magnetic resonance in the dielectric layers [17,32]. However, for those wavelengths shorter than 800nm, weak magnetic field is concentrated at the edges of the designed structure without any strong enhancement of the magnetic field occurring inside the designed structure, and therefore the energy is absorbed from the top to the bottom of the designed absorber without exhibiting any slow light modes in this case.

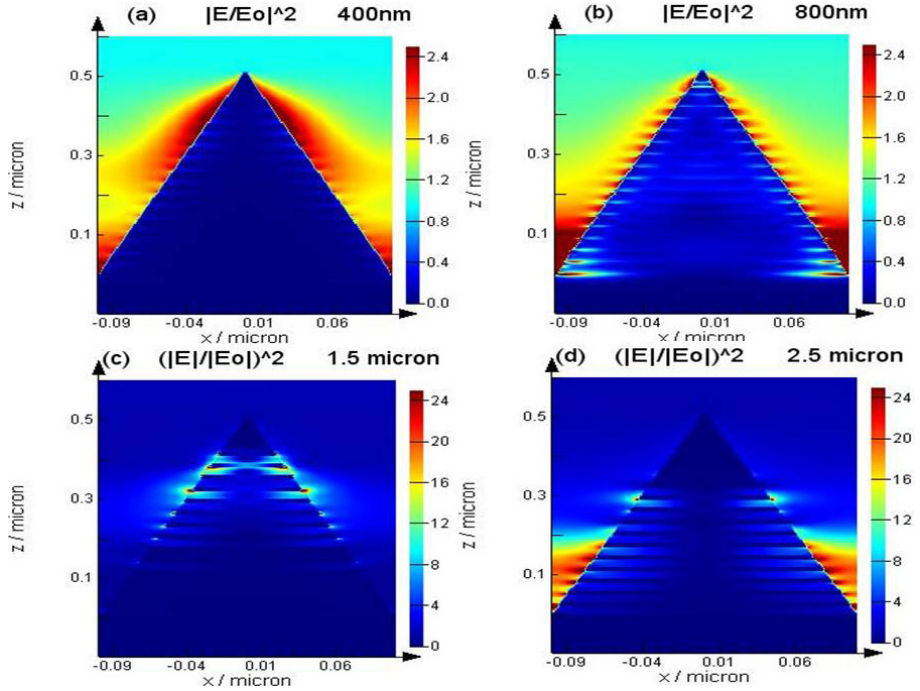

Fig. 4. Distributions of the electric field ($|E/E_0|^2$) of the metamaterial-based nanopyramidal solar energy absorber in the plane $y = 0$ at four different TM waves λ_0: (a) 400 nm, (b) 800 nm, (c) 1.5 μm, and (d) 2.5 μm, respectively. The incident wavelength for each case is shown at the top right side of each figure.

In addition, the distributions of electric field ($|E/E_0|^2$) at different wavelengths (400 nm, 800 nm, 1.5 μm, and 2.5 μm) with TM polarization were also studied. It is obvious from Fig. 4 that oscillating electric field is greatly enhanced and localized at the both edges of the proposed absorber between two adjacent unit cells. Interestingly, for shorter wavelength such as 400nm, the electric field is concentrated at the top of the nanopyramid with relatively low enhancement, and for the longer wavelength such as 800 nm, the weak electric field enhancement occurs in the whole material-based nanopyramid absorber from top to the bottom of the absorber. This can be explained by the graded refractive index (moth eye effects). In comparison, the localized enhancement of the electric field is much more obvious and stronger (dramatically enhances about 10 times (from 2.5 to 25)) in the waveband ($\lambda_0 >$ 800 nm) where the dielectric nanopyramidal structure performs worse. For those wavelengths larger than 800 nm, the strong enhancement of the electric field is excited from the middle to the bottom of the designed absorber with the increase of the wavelength. Obviously, this is due to the localized surface plasmon resonance excited in the metal/dielectric interface [33]. And the electric field enhancement effect is the strong coupling of the incident light with the surface plasmonic mode. Thus, the energy of the incoming wave is fully transferred to surface plasmon oscillation and evanescent electromagnetic field. Moreover, the strong enhancement of the electric field indicates the strong charge accumulation at these sites. This can be observed from the distributions of the electric field ($|E/E_0|^2$), the y-component of the electric field ($|E_y|^2$), and the z-component of the electric field ($|E_z|^2$) in the metal/dielectric interface

#190965 - $15.00 USD Received 24 May 2013; revised 11 Jul 2013; accepted 11 Jul 2013; published 29 Jul 2013

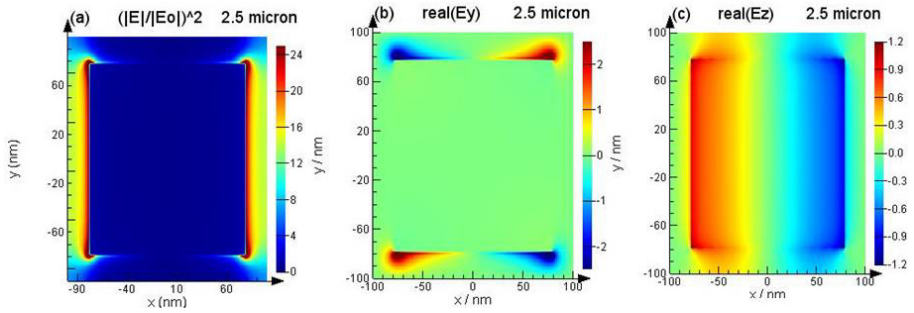

Fig. 5. Distributions of (a) the electric field ($|E/E_0|^2$); (b) the y-component electric field (real (Ey)); (c) the z-component electric field (real (Ez)) of the metamaterial-based nanopyramidal solar energy absorber in the metal/dielectric interface (z = 110 nm plane) at the TM wave λ_0 = 2.5 μm for the metamaterial-based nanopyramidal solar energy absorber. The incident wavelengths are shown at the top right side of each figure.

shown in Fig. 5 (here only shows the plane of z = 110 nm and λ_0 = 2.5 μm as an example) and the z-component of the electric field ($|E_z|^2$) in the plane y =0 at wavelengths of 1.5 μm and 2.5 μm depicted in Figs. 6(a) and 6(b). The opposite charges accumulating at the edges of the metal film indicate the excitation of electric dipole resonance in the metal film.

Therefore, the local electrical field is strongly enhanced, contributing to the resonance absorption in the designed absorber. As the width of the meta-nanopyramid increases, the resonance wavelength increases. That is to say, the resonance wavelength is approximately proportional to the width of the meta-nanopyramid, which is in accordance with the description in [16,17,34].

Furthermore, to gain a deep insight into the nature of the electric and magnetic resonances, the current density (J) distributions at the wavelengths of λ_0 = 1.5 μm and 2.5 μm were calculated (depicted in Figs. 6(c) and 6(d) by the color maps). Due to the metal film thickness is of the same magnitude as the skin depth, the interaction between the electric field components on both surfaces leads to the well-known symmetric and anti-symmetric surface mode. This can be observed from Figs. 6(c) and 6(d), where the symmetric currents and anti-symmetric currents (depicted in Figs. 6(c) and 6(d) by the black arrows) are formed in the metal layers and strong enhancement of electric and magnetic fields is excited. Symmetric current indicates the occurrence of the electronic resonance in the designed absorber, while anti-symmetric current induced in the adjacent metal layers forms a circular current, and thus gives rise to a magnetic dipole response and the magnetic resonance in the dielectric layers [35,36]. Therefore, the proposed solar energy absorber exhibits both the electric and magnetic resonances.

#190965 - $15.00 USD Received 24 May 2013; revised 11 Jul 2013; accepted 11 Jul 2013; published 29 Jul 2013

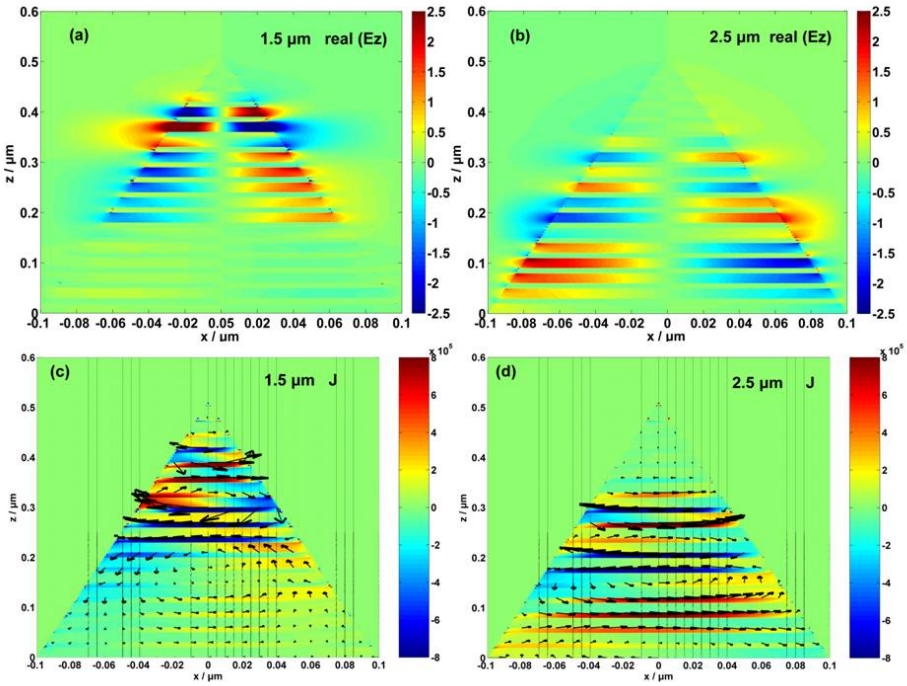

Fig. 6. Distributions of the *z*-component electric field (real (E_z)) of the metamaterial-based nanopyramidal solar energy absorber in the plane $y = 0$ at two TM waves λ_0: (a) 1.5 μm, and (b) 2.5 μm, respectively. Current density (J) distributions (color maps) and current flow directions (arrow maps) in the plane $y = 0$ at two different TM waves λ_0: (c) 1.5 μm, and (d) 2.5 μm, respectively. The incident wavelength for each case is shown at the top right side of each figure.

4. Conclusions

In summary, an efficient solar energy absorber based on metamaterial is proposed and numerically studied. The proposed absorber has a very high absorption performance in the entire solar spectrum with wide receiving angle, omni-direction and polarization-independence and thus can dramatically improve the efficiency of the solar light absorbing. The metamaterial-based nanopyramidal solar energy absorber can obtain near unity absorption in the waveband where the dielectric nanopyramid absorber also performs well, which is mainly due to the graded refractive index (moth eye effects) and the absorption results from the electric field coupled resonance is weak. In contrast, in the waveband where the dielectric nanopyramid absorber performs worse, the designed meta-pyramidal absorber still works well and exhibits both the electric and magnetic resonance light trapping effects and thus to effectively couple, harvest and absorb the solar energy. This is due to the incoming light energy is fully transferred to the surface plasmon oscillation, magnetic oscillation, and evanescent electromagnetic field. It is worth mentioning that the metamaterial-based nanocone shape or nanoparabola shape solar absorbers have similar phenomena. By adjusting the geometrical parameters of the multiple-layer pyramidal structure, one can obtain efficient broadband absorption in other waveband. The designed structure could be fabricated by combining the electron-beam lithography (or interference lithography, focus-ion beam milling) with vacuum coating equipment and Ion beam etching technology. This work provides an effective way to construct broadband solar energy absorber with high absorption in stealth technology and also a theoretical support for the ongoing experiment. Moreover, the meta-nanopyramid array can be used as solar thermal collector. After the light is absorbed by the meta-nanopyramid array, the light energy will be converted

#190965 - $15.00 USD Received 24 May 2013; revised 11 Jul 2013; accepted 11 Jul 2013; published 29 Jul 2013

to heat. The heat can be stored or can be used to generate electricity or to heat water for the further use.

Acknowledgments

This work is supported by the Ministry of Science and Technology of China under grant number 2010DFR10660. The Financial support from the 100 Talents Program of Chinese Academy of Sciences is also acknowledged.

#190965 - $15.00 USD Received 24 May 2013; revised 11 Jul 2013; accepted 11 Jul 2013; published 29 Jul 2013